Molecular Cell, Vol. 16, 425–438, November 5, 2004, Copyright ©2004 by Cell Press

Structural Basis for Androgen Receptor Interdomain and Coactivator Interactions Suggests a Transition in Nuclear Receptor Activation Function Dominance

Bin He,[1,2,3,9] Robert T. Gampe, Jr.,[7] Adam J. Kole,[7,8] Andrew T. Hnat,[1,3] Thomas B. Stanley,[5] Gang An,[5] Eugene L. Stewart,[6] Rebecca I. Kalman,[1,3] John T. Minges,[1,3] and Elizabeth M. Wilson[1,2,3,4,*]

[1]Laboratories for Reproductive Biology
[2]Lineberger Comprehensive Cancer Center
[3]Department of Pediatrics
[4]Department of Biochemistry and Biophysics
University of North Carolina at Chapel Hill
Chapel Hill, North Carolina 27599
[5]Gene Expression and Protein Biochemistry
[6]Computational Chemistry
[7]Structural Sciences
Discovery Research
GlaxoSmithKline
Research Triangle Park, North Carolina 27709
[8]Department of Chemistry
Duke University
Durham, North Carolina 27710

Summary

The androgen receptor (AR) is required for male sex development and contributes to prostate cancer cell survival. In contrast to other nuclear receptors that bind the L*XX*LL motifs of coactivators, the AR ligand binding domain is preferentially engaged in an interdomain interaction with the AR F*XX*LF motif. Reported here are crystal structures of the ligand-activated AR ligand binding domain with and without bound F*XX*LF and L*XX*LL peptides. Key residues that establish motif binding specificity are identified through comparative structure-function and mutagenesis studies. A mechanism in prostate cancer is suggested by a functional AR mutation at a specificity-determining residue that recovers coactivator L*XX*LL motif binding. An activation function transition hypothesis is proposed in which an evolutionary decline in L*XX*LL motif binding parallels expansion and functional dominance of the NH_2-terminal transactivation domain in the steroid receptor subfamily.

Introduction

Nuclear hormone receptors (NRs) are transcriptional activators that regulate hormone-dependent differentiation (Tsai and O'Malley, 1994; Chawla et al., 2001) and increase gene activity by recruiting coactivators that assist in chromatin remodeling (Glass and Rosenfeld, 2000). Steroid receptors, a subgroup of the NR superfamily, have two predominant activation regions. Activation function 1 (AF1) in the NH_2-terminal region is variable in sequence and its activity is receptor and cell-type dependent (Metzger et al., 1992; Tremblay et al., 1999). Activation function 2 (AF2) in the ligand binding domain (LBD) is a highly conserved hydrophobic cleft flanked by opposing charge residues (Webster et al., 1989; Nolte et al., 1998; He and Wilson, 2003) that binds the L*XX*LL motifs of the steroid receptor coactivator (SRC) family of coactivators (Onate et al., 1995; Hong et al., 1996; Voegel et al., 1998). Some coactivators and associated complexes such as p300/CBP have potent histone acetyl transferase activity (Ogryzko et al., 1996). Hormone binding regulates these activities by repositioning helix 12 to complete the AF2 binding surface (Moras and Gronemeyer, 1998).

Sequence conservation of NR AF2 reflects a common function of coactivator binding. The androgen receptor (AR) AF2 has weak activity in mammalian cells but recruits SRC coactivators when highly expressed as in recurrent prostate cancer (Gregory et al., 2001). AR AF2 preferentially binds the F*XX*LF motif in the AR NH_2-terminal region (He et al., 2000) and AR coregulatory proteins (He et al., 2002b; Hsu et al., 2003). Interaction of the AR F*XX*LF motif ^{23}FQNLF^{27} with AF2 is androgen dependent and mediates the NH_2- and carboxy (C)-terminal (N/C) interaction (Langley et al., 1998). An additional NH_2-terminal W*XX*LF binding motif ^{433}WHTLF^{437} contributes to the N/C interaction by binding AF2 (He et al., 2002a). These interdomain interactions are important in regulating some but not all androgen-dependent genes in transient reporter assays.

Here we report the molecular basis for F*XX*LF and L*XX*LL motif binding to AF2 based on a comparison of peptide bound and peptide-free AR LBD crystal structures and site-directed mutagenesis. We demonstrate that AR 20-30 F*XX*LF and TIF2-III 740-753 L*XX*LL motifs bind AR AF2, but only the F*XX*LF motif peptide binds with an intact primary charge clamp and better recognition conferring hydrophobic contacts than does the L*XX*LL motif. Shown are key residues that differentiate F*XX*LF motif binding and a functional AR mutation in prostate cancer that recovers L*XX*LL motif binding. The data suggest a transition in dominant transactivation domains from AF2 to AF1 during NR evolution.

Results

AR F*XX*LF Peptide-AR LBD-R1881 Structure

Human AR LBD bound to R1881 was cocrystallized with human AR F*XX*LF peptide 20-30, TIF2 coactivator L*XX*LL peptide 740-753, and without peptide. The resulting monomeric structures contain 12 α helices and 4 small β strands assembled into the familiar 3-layer α-helical structure (Figures 1A and 1B). The arrangement resembles structures of the progesterone receptor (PR) (Williams and Sigler, 1998), glucocorticoid receptor (GR) (Bledsoe et al., 2002), AR (Matias et al., 2000; Sack et al., 2001), and other NRs (Gampe et al., 2000). R1881 is bound in the ligand binding pocket in a mode consistent with that of Matias et al. (2000). The characteristic A- and D ring hydrogen (H) bonding network and other key interactions are maintained.

*Correspondence: emw@med.unc.edu
[9]Present address: M533 DeBakey Building, Department of Molecular and Cellular Biology, Baylor College of Medicine, One Baylor Plaza, Houston, Texas 77030.

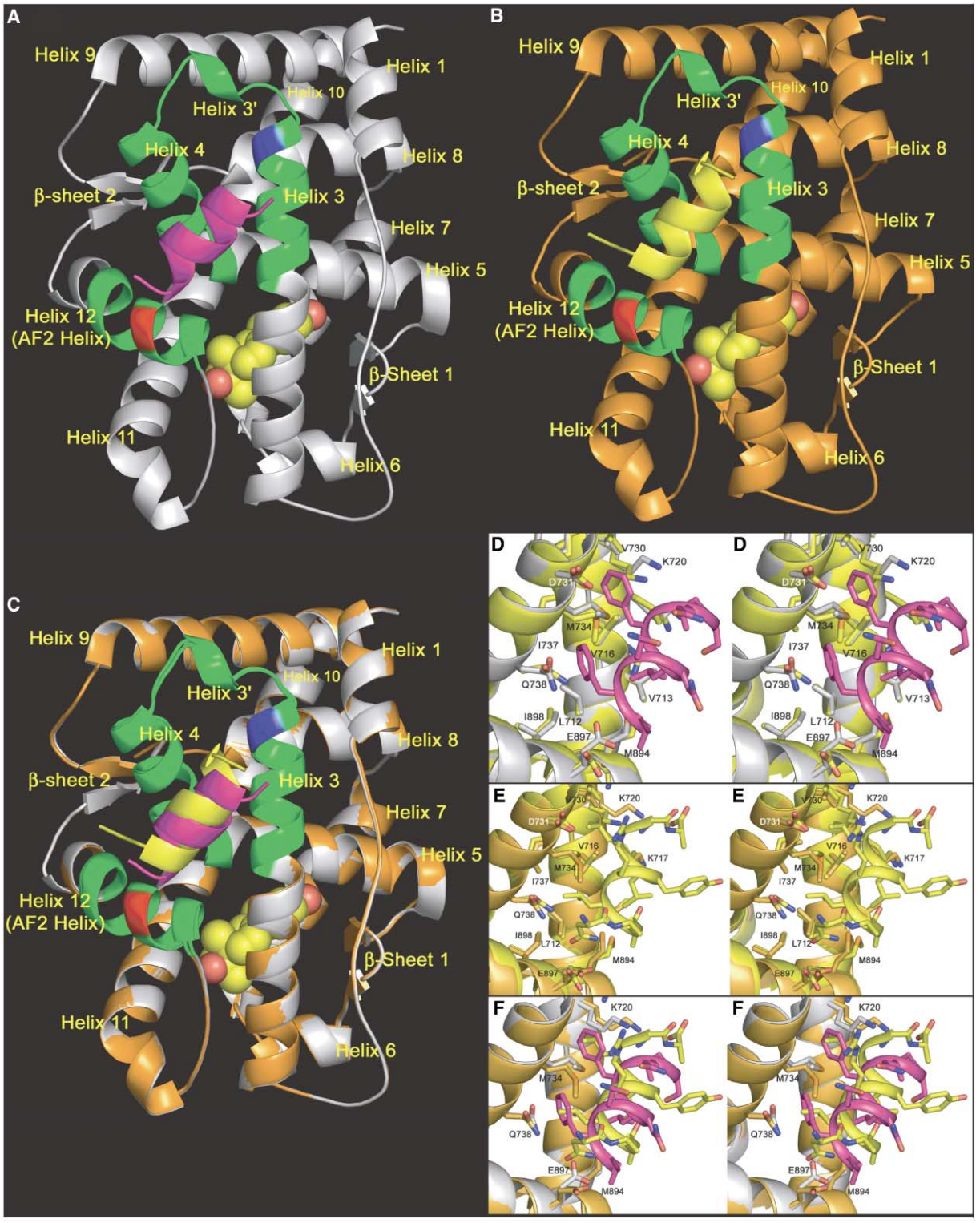

Figure 1. Structures of the AR F*XX*LF and TIF2-III L*XX*LL Peptides Bound to AR-R1881

(A) Global architecture of AR 20-30 F*XX*LF (magenta ribbon) and R1881 (space filled atoms yellow carbon and red oxygen) bound to AR LBD (gray ribbon) with helices 3, 3′, 4, and 12 (green ribbon) in AF2. Conserved charge-clamp residues are K720 (blue) in helix 3 and E897 (red) in helix 12.

(B) Global architecture of TIF2-III 740-753 L*XX*LL (yellow ribbon) and R1881 (as in [A]) bound to AR LBD (orange ribbon) with helices 3, 3′, 4, and 12 (green ribbon) in AF2.

(C) A ~2.0 Å C-terminal shift of bound TIF2-III (yellow ribbon) relative to bound AR F*XX*LF (magenta ribbon) by superimposition of (A) and (B) (backbone root-mean-square distance [rmsd] 0.21 Å).

Table 1. Crystallographic Data and Refinement Statistics

Crystals	AR R1881 AR20-30	AR R1881 TIF2-III	AR R1881 None
X-ray source	Rigaku-RU-H2R-200	APS-32ID	APS-17ID
Space group	$P2_12_12_1$	$P2_12_12_1$	$P2_12_12_1$
Unit cell	a = 54.9, b = 66.1, c = 70.4	a = 54.6, b = 66.7, c = 69.4	a = 56.9, b = 65.8, c = 72.6
Resolution (Å)	50.0–1.8	50.0–1.9	50.0–2.3
Unique reflections	22,123	20,036	13,364
Completeness (%)	90.4	93.0	99.4
I/σ (last shell)	37.8 (2.1)	30.0 (4.7)	32.0 (2.7)
R_{sym}[a] (%)	4.1	7.3	5.7
Refinement			
Resolution range	50.0–1.8	50.0–1.9	50.0–2.3
R factor[b] (%)	21.0	22.1	21.5
R_{free} (%)	21.3	24.1	24.2
Rmsd bond lengths (Å)	0.007	0.006	0.007
Rmsd bond angles (°)	1.1	1.1	1.1
Total nonhydrogen atoms	2,267	2,185	2,086
Accession numbers	1XOW	1XQ2	1XQ3

Rmsd is the root-mean-square deviation from ideal geometry.
[a] $R_{sym} = \Sigma|Iavg - Ii|/\Sigma Ii$
[b] R factor = $\Sigma|F_P - F_{Pcalc}|/\Sigma F_p$, where F_p and F_{pcalc} are observed and calculated structure factors; R_{free} was calculated from a random set of reflections that were excluded from refinement and R factor calculations.

Excellent quality electron density accounts for AR F*XX*LF residues 21–30 (Figure 2A and Table 1) and is clearly visible as a two-turn amphipathic α helix where F23, L26, and F27 are directed toward the LBD surface and Q24, N25, and Q28 are exposed to the solvent (Figure 2C). FQNLF is H bonded NH_2- to C-terminal by the conserved oxy-steroid E897 (helix 12) and K720 (helix 3), respectively, which reside in clusters of opposite charge (He and Wilson, 2003). This result is reminiscent of the charge clamp originally revealed in the SRC-1-PPARγ (Nolte et al., 1998) and other coactivator bound NR structures (Darimont et al., 1998; Shiau et al., 1998; Gampe et al., 2000). Two H bonds are observed between the E897 carboxylate and A22 and F23 amides. Backbone carbonyl oxygens from F27 and V30 H bond with the side chain of K720 (Figure 2A). No interactions are observed from other residues that reside in either charge cluster. Between the charge clusters, ten mostly hydrophobic residues from helices 3, 4, and 12 form the AF2 cleft floor (I898, L712, I737, and V716, Figure 2F), which is bounded on one side by a low rise from M894, V713, and K717, and on the other by a helix 4 ridge from Q738, M734, V730, and Q733. Binding F*XX*LF increases the distance between M734 and M894 by ~1.5 Å, allowing extensive hydrophobic exposure through face on interactions from the F23 and F27 phenyl rings with the helix 4 ridge of the AF2 cleft (Figures 2C and 2F). Both F23 and F27 adopt similar conformers and lie in a staggered, almost parallel orientation near M734 that allows the planar aromatic ring of F23 to contact the Q738 side chain (carbons Cγ and Cδ) and be enclosed by L712, V716, M734, I737, M894, I898, and L26. All F23 aromatic side chain atoms lie between 3.5 and 3.9 Å of the Q738 Cδ and Cγ carbons. The planar aromatic ring of F27 contacts the Cγ carbon and Sδ sulfur of M734 and the K720 Cδ and Cε carbons and is enclosed by V716, V730, Q733, and I737. All F27 aromatic side chain atoms lie between 3.4 and 4.0 Å of the M734 side chain, with additional hydrophobic contact between the L26 side chain and V713, V716, and M894 from helix 12.

Superimposition of backbone heavy atoms indicates no major rearrangement of the protein backbone or ligand binding pocket with F*XX*LF binding. However, consistent with an induced fit mechanism, F*XX*LF causes conformational changes in AR side chains contacting the peptide (Figure 1D). Charge-clamp residues K720 and E897 move and form H bonds with the peptide. Side chain interactions between Q738 and F23 induce conformational changes in V716 and in the flexible M734. An increased distance from 3.0 to 3.9 Å between Q738 Oε1 and Q902 Nε2 suggests Q738 and F23 interactions disrupt a H bond network from Q738 to Q902 and K905 in helix 12 that was observed in the peptide-free structure. At the start of helix 4, V730 is drawn closer to F27. Combined interactions of F27 and the F*XX*LF C-terminal backbone force K720 toward R726, whose guanadinium group moves 4 Å away from its location in the peptide-free structure (Figures 2C and 2F). A change of this magnitude may be driven in part by contact between R726 and an adjacent molecule in the crystal. In helix 12, M894 moves to contact L26 of ^{23}FQNLF^{27}. We conclude that M734, M894, E897, and

(D) Stereoview of AR AF2 showing conformational differences in AR 20-30 bound and unbound states. Amino acid residues of AR (gray)-R1881-F*XX*LF (magenta) and AR (yellow)-R1881 without peptide are superimposed (backbone rmsd 0.21 Å).
(E) Stereoview of AR AF2 showing conformational differences in TIF2-III 740-753 bound and unbound states. Amino acid residues for AR (orange)-R1881-L*XX*LL (yellow) and AR (yellow)-R1881 without peptide structures are superimposed (backbone rmsd 0.20 Å).
(F) Superimposed stereoview of AR AF2 from AR F*XX*LF (magenta)-AR (gray)-R1881 and TIF2-III (yellow)-AR (orange)-R1881 structures (backbone rmsd 0.21 Å). The C-terminal shifted TIF2-III fails to H bond with E897 and forces a conformational change on K720. TIF2-III L745 and L749 Cδ2 carbons occupy similar space to AR 20-30 F23 and F27 but fail to establish extensive hydrophobic contact afforded by F23 and F27.

K720 play a prominent role in AR F*XX*LF binding and undergo notable conformational change along with R726 that does not contact the peptide (Figure 1A, 2C, and 2F).

TIF2 L*XX*LL Peptide-AR LBD-R1881 Structure

Good quality electron density defines the bound TIF2-III 740–753 peptide as a two-turn amphipathic α helix with L745, L748, and L749 turned toward the LBD surface and R746 and Y747 exposed to the solvent (Figures 1B and 2D, and Table 1). Backbone amides of TIF2-III ^{745}LRYLL^{749} are too distant to H bond with the disordered carboxylate oxygen atoms of AR E897 in helix 12 or other residues in the negative charge cluster (Figures 2B and 2D). Lack of an NH_2-terminal backbone H bond to the charge-clamp residue distinguishes L*XX*LL binding to AR from previously described coactivator bound NR structures. Disorder in the E897 carboxylate oxygens also prevents defining a stable electrostatic interaction to the proximal TIF2-III N742 Nδ2, which further H bonds to Nϵ2 of AR Q738 and participates in the H bond network to helix 12 Q902 and K905 described above. On the C-terminal end of L*XX*LL, the backbone carbonyls of L748, L749, and K751(A) accept a H bond from AR K720 Nζ. The side chain of AR R726 moves to strongly H bond (2.6 Å) with the AR Q733 side chain and weakly (3.5 Å) with the TIF2-III L749 carbonyl. Ten residues in helices 3, 4, and 12 interact with the branched leucine side chains in TIF2-III. Both TIF2-III L745 and L749 adopt similar conformers and lie in a staggered almost parallel orientation near AR M734. Since fewer side chain atoms from the branched TIF2-III L745 and L749 are directed toward the helix 4 ridge, fewer hydrophobic contacts are made. The single Cδ2 methyl of L745 makes only two contacts with the AR Q738 side chain at Cγ (3.3 Å) and Cδ (3.5 Å) and is enclosed by AR V716, M734, and M894. Likewise, TIF2-III L749 Cδ2 makes two contacts (3.9 Å) with AR M734 Cγ and Sδ and is enclosed by AR K720, V730, and I737. Additional hydrophobic contact occurs between the TIF2-III L748 side chain and AR M894 in helix 12 and is enclosed by AR V716 and V713.

Like F*XX*LF, L*XX*LL peptide binding does not impose large changes in the global structure, but induces conformational changes in AR side chains that contact or lie near the peptide (Figures 1B, 1E, and 2D). Slight movement in AR E897 may arise from the adjacent TIF2-III N742 side chain since it is too distant to H bond to the peptide backbone. On the other end, AR K720 rearranges to H bond with TIF2-III L748, L749, and the C terminus. A movement of $\sim$2.0 Å is observed for AR R726 as it forms interactions with TIF2-III L749 and AR Q733 (Figure 2) similar to the secondary charge clamp described for GR (Bledsoe et al., 2002). However, 3.5 Å between the AR R726 side chain and TIF2-III L749 backbone oxygen indicates a weak H bond, and 4.4 Å between TIF2-III R746 and AR D731 is too distant for a second direct H bond. Thus, these interactions do not qualify as a fully intact secondary charge clamp. A moderate change in the flexible AR M734 side chain is seen as the Cδ2 methyls from L745 and L749 make contact with M734. TIF2-III L745 induces a slight change in AR Q738 and M894 side chains. M734, Q738, M894, K720, and in particular R726, contribute to binding the TIF2-III peptide and undergo notable conformational change (Figures 1E, 2D, and 2F).

Superimposition of the AR structures illustrates similarities and differences between the AR 20-30 and TIF2-III binding modes (Figures 1C, 1F, and 2E). Both amphipathic peptides align along a similar helical axis and shelter hydrophobic residues within the AF2 cleft. However, a $\sim$2.0 Å C-terminal shift along the helical axis for TIF2-III relative to AR20-30 is observed, separating TIF2-III from charge-clamp residue AR E897 and preventing H bonding. The sizeable shift and resulting absence of H bonding distinguishes TIF2-III from AR 20-30 motif binding to the AR LBD. TIF2-III induces conformational changes where AR K720 is pushed away relative to the F*XX*LF and peptide-free structures and R726 contributes a new distant H bond to the TIF2-III L749 backbone oxygen and a closer one to the AR Q733 side chain. Despite the sizeable shift of L*XX*LL, the respective i+1, i+4, and i+5 leucine residues appear in register and respectively contact many of the same residues as F*XX*LF. However, these contacts are fewer and less optimized due to the geometry and conformation of the branched leucine side chains in relation to the AF2 surface.

Determinants of AF2 Binding Specificity

Consistent with previous cell-based and in vitro binding studies (He et al., 2001; He and Wilson, 2003), the AR LBD binds AR 20-30 F*XX*LF (9.2 $\pm$ 0.4 μM) with higher affinity than the L*XX*LL peptide TIF2-III 740-751 (78 $\pm$ 28 μM) determined by fluorescence polarization (Figures 3A and 3B). In contrast, ERα LBD preferentially binds the L*XX*LL peptide (2.1 $\pm$ 0.2 μM) over the F*XX*LF peptide (>100 μM).

Crystal structures and comparative sequence alignment (Figure 3C) suggest V730 and M734 discriminate F*XX*LF and L*XX*LL binding. AR-V730I-M734I that mimics PR AF2 and AR-V730L-M734V that mimics ERα AF2 decrease binding of the AR F*XX*LF peptide (Figure 3D). The ERα-like mutant also decreases binding of F*XX*LF sequences from coregulatory proteins ARA54 and ARA70 (Figure 3E). In contrast, both mutants increase AR binding of the TIF2-III and SRC1-IV L*XX*LL peptides (Figure 3D).

An effect of V730 and M734 on AR F*XX*LF binding was also evident in transcription assays using PSA-Enh-Luc (Huang et al., 1999) and p21-Luc (Lu et al., 1999) that require the AR N/C interaction for maximal gene activation, with $\sim$90% loss of activity by the AR-^{23}F*XX*AA^{27} mutant (Figures 4A and 4B). The PR-like and ERα-like AR mutants reduce androgen-dependent transactivation of these reporters but cause little change in MMTV-Luc, a reporter less dependent on the AR N/C interaction (He et al., 2002a). The results support AR AF2 residues V730 and M734 are critical for F*XX*LF motif binding.

Ligand Dissociation Rates Support the Role of M734 in F*XX*LF Motif Binding

Mutations that disrupt the AR N/C interaction exhibit reduced half-times ($t_{1/2}$) of androgen dissociation (He et al., 2000, 2001). [^{3}H]R1881 dissociation from the PR-like mutant AR-V730I/M734I ($t_{1/2}$ = 72 $\pm$ 11 min; K_d = 0.71 $\pm$ 0.28 nM) and ERα-like mutant AR-V730L/M734V ($t_{1/2}$ =

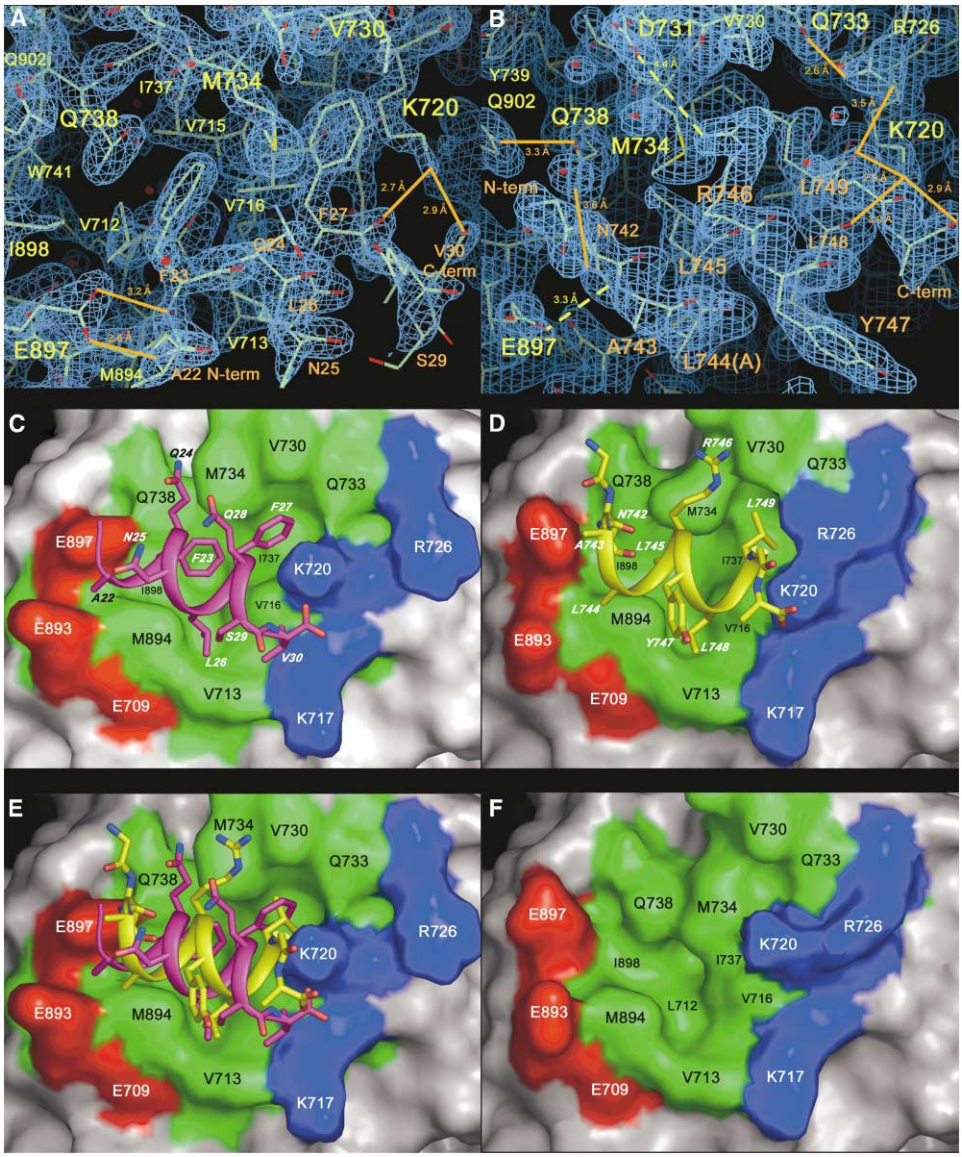

Figure 2. Structural Details for AR FXXLF and TIF2-III LXXLL Peptide-AR LBD-R1881 Complexes

(A) $2F_o - F_c$ electron density map (blue) contoured at 1.8σ from 1.8 Å data for bound AR 20-30. Except for NH_2-terminal arginine, clearly ordered electron density is observed for all peptide residues. Carbon atoms are green, oxygen red, and nitrogen blue; annotations for AR LBD are in yellow, AR 20-30 in orange with intact charge-clamp H bonds in solid orange lines with distances.

(B) $2F_o - F_c$ electron density map (blue) contoured at 1.4σ from 1.9 Å data for bound TIF2-III 740-753. Electron density is devoid for K740, D752, and D753 and poor for L744 and K751 that were built as alanine. H bond interactions are shown with solid orange lines. Excess distance and/or the disordered E897 carboxylate oxygens prevent description of electrostatic interactions to the TIF2-III backbone amides and the proximal N742 side chain. Also the D731 to TIF2-III R746 distance is too long to support direct H bonding (dashed yellow lines with distances and colors as in [A]).

(C) Surface representation of AR AF2 with bound AR 20-30. AR E897, E893, and E709 with K720, K717, and R726 (Roman font) create charge clusters (positive in blue, negative in red) that flank FQNLF (italicized font). F*XX*LF is charge clamped by E897 and K720.

(D) Surface representation of AR AF2 bound to TIF2-III. AR E897, E893, and E709 and K720, K717, and R726 (Roman font) create charge clusters (positive blue, negative red) that flank LRYLL (italicized font). TIF2-III lacks backbone H bonds to AR E897 but H bonds with K720 and AR R726 that moves left to weakly H bond with L749. TIF2-III L745 and L749 make fewer less optimal hydrophobic contacts with Q738, M734, and V730 located in AF2 (green) helix 4 ridge and K720 as does L748 to AR V713.

(E) Superimposed surface representation of the C-terminal shift of TIF2-III (yellow) to the AR F*XX*LF (magenta)-AR-R1881 structure (backbone rmsd 0.21 Å). TIF2-III LRYLL i+1 (not visible) and i+5 leucines are shifted but in register with corresponding phenylalanines in AR 20-30. Binding TIF2-III requires AR K720 to move (Figure 2D) allowing AR R726 to move and participate in L*XX*LL binding.

(F) Surface representation of peptide-free AR AF2. AR E897, E893, E709 and K720, K717, R726 present negative (red) and positive (blue) charge clusters that flank AF2 (green).

71 ± 7 min; K_d = 1.4 ± 0.63 nM) was faster than from wild-type AR ($t_{1/2}$ = 109 ± 11 min; K_d = 0.52 ± 0.08 nM) (Figure 4C) even though equilibrium binding affinities were not altered. A similarly fast dissociation rate from AR-M734I ($t_{1/2}$ = 75 ± 7 min; K_d = 0.75 ± 0.09 nM) indicates M734 is critical for F*XX*LF motif binding.

A Functional AR Mutation in Prostate Cancer at Specificity-Determining Residue V730

V730M is a functional somatic mutation that increases AR transactivation by adrenal androgens (Culig et al., 1993; Peterziel et al., 1995). Because mutations at V730 to longer side chain residues increase L*XX*LL motif binding (Figure 3D, data not shown), we tested whether a functional mutation at this site alters binding specificity and coactivator recruitment. We found the interaction between AR-V730M and GAL-SRC1-IV increases compared to wild-type AR in the presence of R1881, dihydrotestosterone (DHT), androstenedione, and androstanediol, but not progesterone (Figures 4D and 4E). The small decrease in F*XX*LF binding agrees with ligand dissociation studies that show AR-V730M ($t_{1/2}$ = 112 ± 22 min; K_d = 0.42 ± 0.15 nM) similar to wild-type AR.

In vitro binding of GST-TIF2 and GST-SRC1 L*XX*LL fragments to ^{35}S-AR-LBD-V730M also increases in the presence of DHT or androstenedione compared to wild-type AR (Figure 4F). But there is no increase in AR-V730M binding of AR F*XX*LF in the presence of DHT. Specificity for F*XX*LF motif binding in the presence of high-affinity androgens is also evident. The results suggest somatic prostate cancer AF2 mutant AR-V730M recovers L*XX*LL binding with minimal effect on F*XX*LF binding.

Declining AF2 Activity in PR, GR, and AR

AR AF2 residue V713 is present in ERα, ERβ, and steroid receptor progenitors in sea lamprey and mollusk, but is replaced by L727 in PR and I572 in GR (Figure 3C). In agreement with the structures, we found that V713 is important for AR binding of the F*XX*LF and L*XX*LL motifs. AR-V713L and AR-V713I mimic PR and GR at this site and reduce binding of AR F*XX*LF and coactivator L*XX*LL motifs (Figure 5A), suggesting selective pressure maintained ancestral V713 for F*XX*LF binding.

Transition of valine to longer chain residues in PR and GR raised the possibility that L*XX*LL binding and AF2 activity decreases during evolution. Based on sequence alignment and crystal structures (Williams and Sigler, 1998), AR AF2 V713, V730, and M734 correspond to PR L727, I744, and I748 and GR I572, L589, and M593 (Figure 3C). Transactivation by GAL-PR-LBD-L727V is greater than wild-type (Figure 5B) and increases with the L727V-I748V mutations that restore both ancestral valines. GAL-GR-LBD-I572V strongly increases transactivation relative to wild-type, as did the corresponding mutant GAL-GR-LBD-I572V-M593V, suggesting that evolving sequence changes in PR and GR decrease inherent activity of AF2. Inserting a set of AR AF2 residues in GAL-PR-LBDm4 and GAL-GR-LBDm6 reduced AF2 activity.

We found that evolving sequence changes in PR and GR that reduce AF2 activity correlate with decreased binding of the SRC coactivators. GAL-PR-LBD-L727V increases SRC/p160 coactivator binding (Figure 5C). The m4 mutant in which four PR AF2 residues are replaced by corresponding residues of AR, increases coactivator binding, but to a lower extent than the single mutant relative to wild-type. Similarly, GAL-GR-LBD-I572V increases coactivator interaction (Figure 5D) as does GAL-GR-LBDm6, but to a lower extent than the single mutant. Evolving AF2 sequence in PR and GR limits inherent transcriptional activity of AF2 by decreasing coactivator recruitment. The decrease is less than that for AR where evolutionary changes favor F*XX*LF binding.

F*XX*LF Motif Binding by PR and GR Mutants

Structural determinants of AF2 binding specificity were tested by attempting to convert PR and GR AF2 into an F*XX*LF binding site. GAL-PR-LBD and VP-AR1-660 do not interact, but GAL-PR-LBD-L727V interacts with this AR NH_2-terminal fragment (Figure 5E) and increases further when AR V713, V730, M734, and I898 replace corresponding PR residues. A similar set of mutations in GAL-GR-LBD-m6 increases binding of VP-AR1-660 compared to wild-type GAL-GR-LBD, and binding is eliminated by the AR F*XX*AA mutation (Figure 5F). The results support M734, V730, and V713 as key residues in AR F*XX*LF motif binding. It is noteworthy that PR-LBDm4 and GR-LBD-m6 retain L*XX*LL binding (Figures 5C and 5D), suggesting additional determinants contribute to binding specificity.

Transition to AF1

Dependence of NR AF1 activity on length of the NH_2-terminal domain was measured using human NR-GAL4 DNA binding domain fusion proteins expressed in HepG2 (Figure 6A). We found an exponential increase in transcriptional activity with NH_2-terminal domain length ($R = 0.99$, $n = 9$), with a similar trend seen in HeLa, CV1, and COS cells (data not shown). The data support that AF1 transcriptional strength increases with NH_2-terminal length as it evolves in the NR family.

Discussion

Molecular Determinants of F*XX*LF and L*XX*LL Motif Binding

Our data indicate that differential binding affinity and specificity are established by distinct electrostatic and hydrophobic interactions revealed in our AR-R1881 crystal structures bound with AR F*XX*LF and TIF2-III L*XX*LL peptides. Through an induced fit mechanism, AR 20-30 contacts E897 with classical charge-clamp H bonding that is absent in the bound TIF2-III. Although new distant contacts form between the TIF2-III and AR, the interactions apparently provide insufficient energy to recover what might arise from close NH_2-terminal backbone H bonds with E897. More importantly, selective high-affinity binding by AR AF2 of phenylalanines at i+1 and i+5 suggests that the hydrophobic character, size, and complementarity contribute a substantial nonpolar binding energy.

The crystal structures show that the AR AF2 solvent-exposed hydrophobic cleft shelters hydrophobic residues of bound amphipathic peptides from the solvent

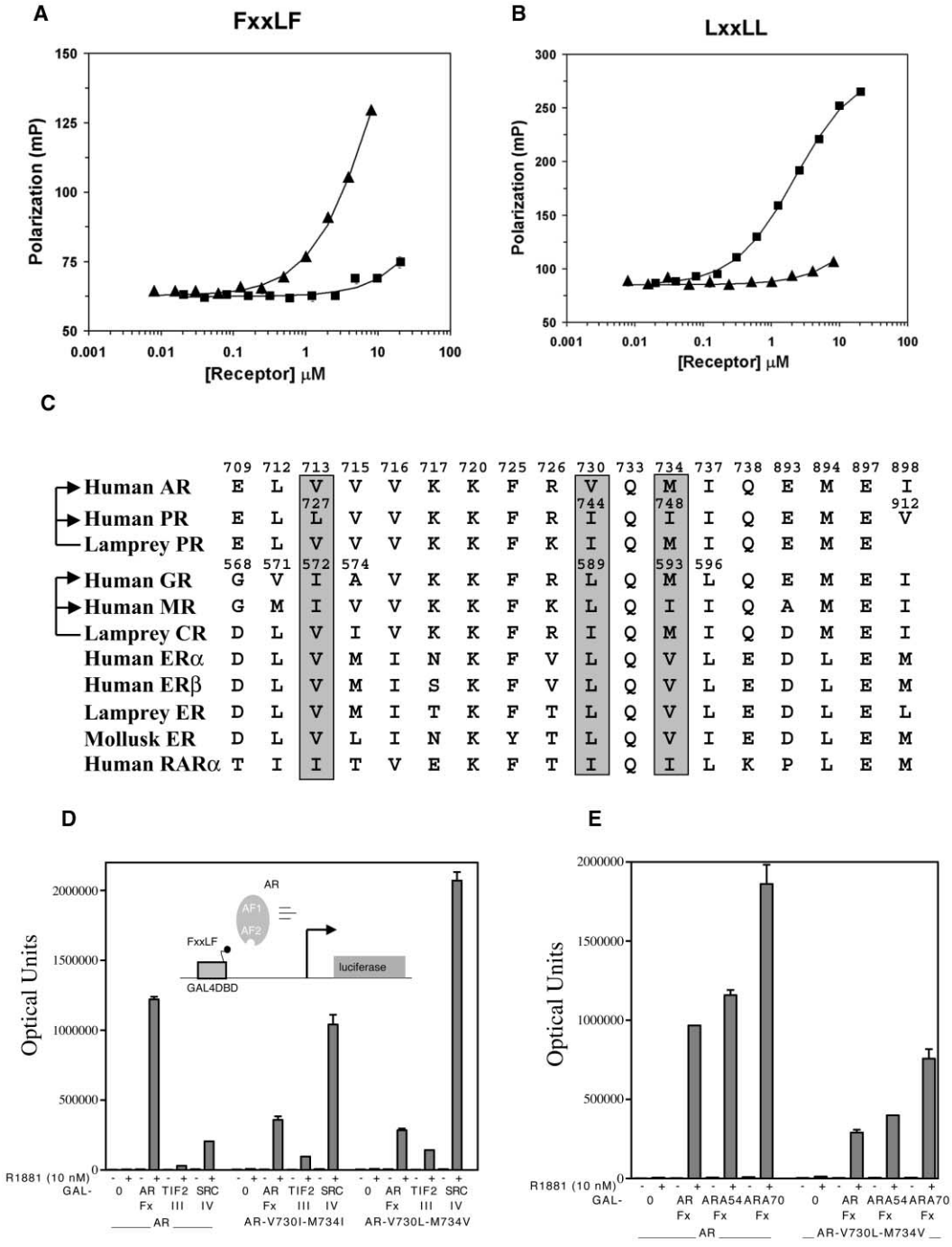

Figure 3. AF2 Determinants of F*XX*LF and L*XX*LL Motif Binding Specificity

(A and B) Affinities of F*XX*LF and L*XX*LL peptides for AR and ERα LBDs. Binding of ERα (■) and AR (▲) LBDs to AR 20-30 ([A], F*XX*LF) and TIF2-III 740-751 ([B], L*XX*LL) and fluoroscein-labeled peptides were measured by fluorescence polarization.

(C) Sequence alignment of AF2 surface residues for human AR GenBank M20132, human PR QRHUP, sea lamprey progestin receptor AY028458, human GR P04150, human mineralocorticoid receptor NP000892, sea lamprey corticoid receptor AY028457, human ERα P03372, human ERβ NP001428, sea lamprey ER AY028456, California sea hare *Aplysia californica* mollusk ER AY327135, and human retinoic acid receptor α P10276. AR AF2 residues involved in F*XX*LF motif binding are shaded.

(D) Substitution of PR and ER residues in AR AF2. Two-hybrid assays in HepG2 cells with and without 10 nM R1881 used 5×GAL4Luc 3 and 10 ng/well pCMVhAR, AR-V730I-M734I, or AR-V730L-M734V, with 50 ng/well of GAL0, GAL-AR20-30 (ARFx), GAL-TIF2-738-756 (TIF2-III, 3rd L*XX*LL), or GAL-SRC1-1428-1441 (SRC-IV, 4th and C-terminal L*XX*LL). Inset: schematic of two-hybrid assay for F*XX*LF motif binding by AR.

(E) Reduction in coregulator F*XX*LF motif binding by ER-like AR mutant. Two-hybrid assays in HepG2 cells with and without 10 nM R1881 used 10 ng/well pCMVhAR or AR-V730L-M734V with 50 ng/well GAL0, GAL-ARFx, GAL-ARA54-447-465 (ARA54Fx), or GAL-ARA70-321-340 (ARA70Fx).

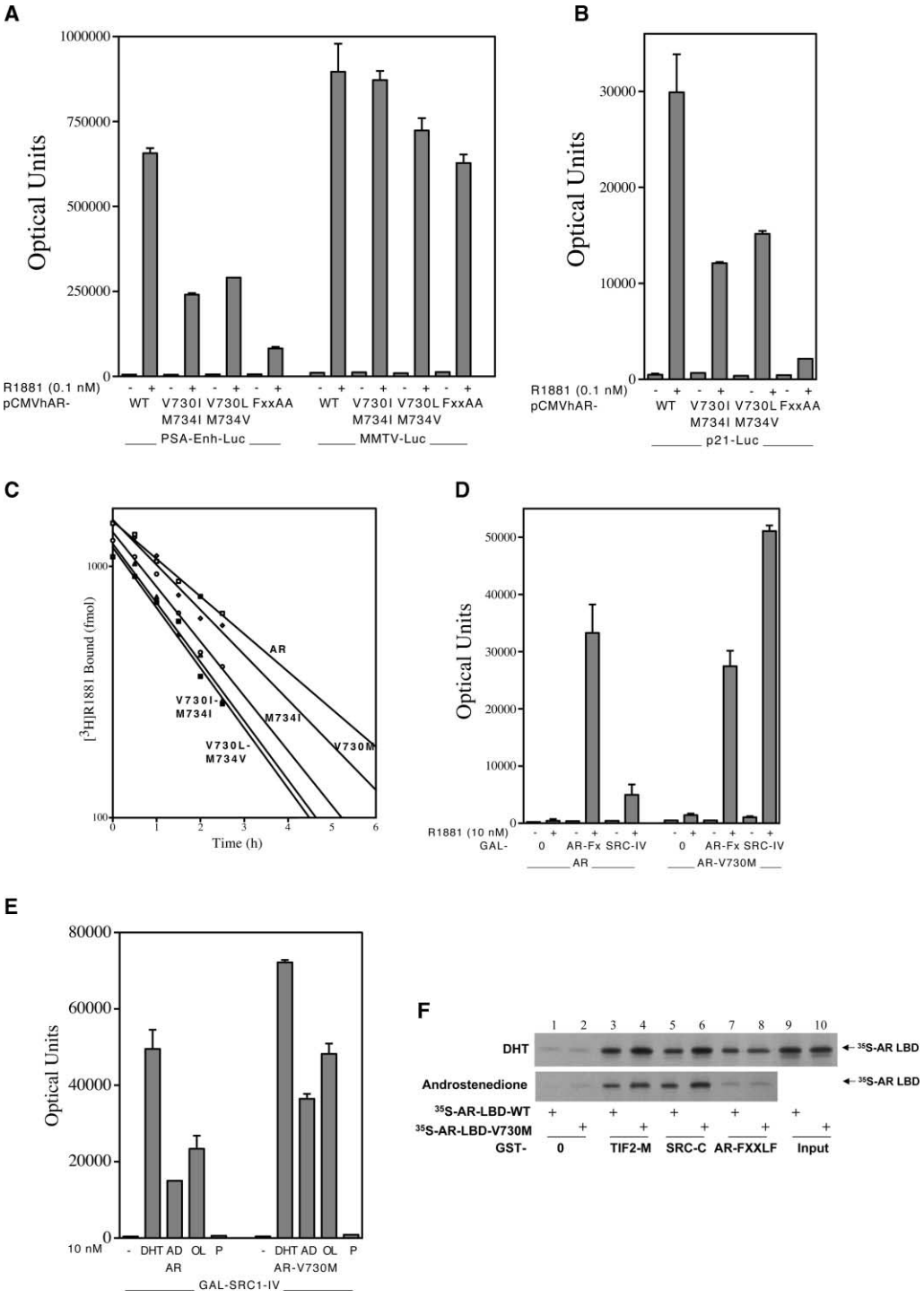

Figure 4. Promoter Dependence and Prostate Cancer Functional Mutant AR-V730M

(A and B) Dependence on the AR NC interaction. Transcriptional activity of AR and mutants was determined in HepG2 cells with and without 0.1 nM R1881 using 50 ng/well pCMVhAR (WT), AR-V730I/M734I, V730L/M734V or L26A/F27A (F*XX*AA) with PSA-Enh-Luc, MMTV-Luc, and p21-Luc.

(C) Reduced AR N/C interaction and increased androgen dissociation. COS cells transfected with pCMVhAR or AR-V730M, M734I, V730I-M734I, or V730L-M734V were incubated with 10 nM [^{3}H]R1881 and dissociation rates measured.

(D) Increase in L*XX*LL binding by prostate cancer AR mutant. Two-hybrid assays in HepG2 cells with and without 10 nM R1881 used 5×GAL4Luc and 10 ng/well pCMVhAR or AR-V730M with 50 ng/well GAL0, GAL-AR20-30 (GAL-ARFx), or GAL-SRC1-1428-1441 (GAL-SRC-IV).

(E) Effects of steroids on L*XX*LL binding. Two-hybrid assays in HeLa cells were performed with and without 10 nM DHT, androstenedione (AD), androstanediol (OL), or progesterone (P) using 50 ng/well GAL-SRC1-IV and 10 ng/well of pCMVhAR or AR-V730M.

(F) Increase in L*XX*LL binding in vitro. Partially purified GST-0, GST-TIF2-624-1141 (TIF2-M), GST-SRC1-1139-1441 (SRC-C), and GST-AR4-52 (AR-F*XX*LF) were incubated with ^{35}S-AR624-919 (WT) and AR-LBD-V730M with and without 1 μM DHT or androstenedione. Input lanes have 30% of the reaction.

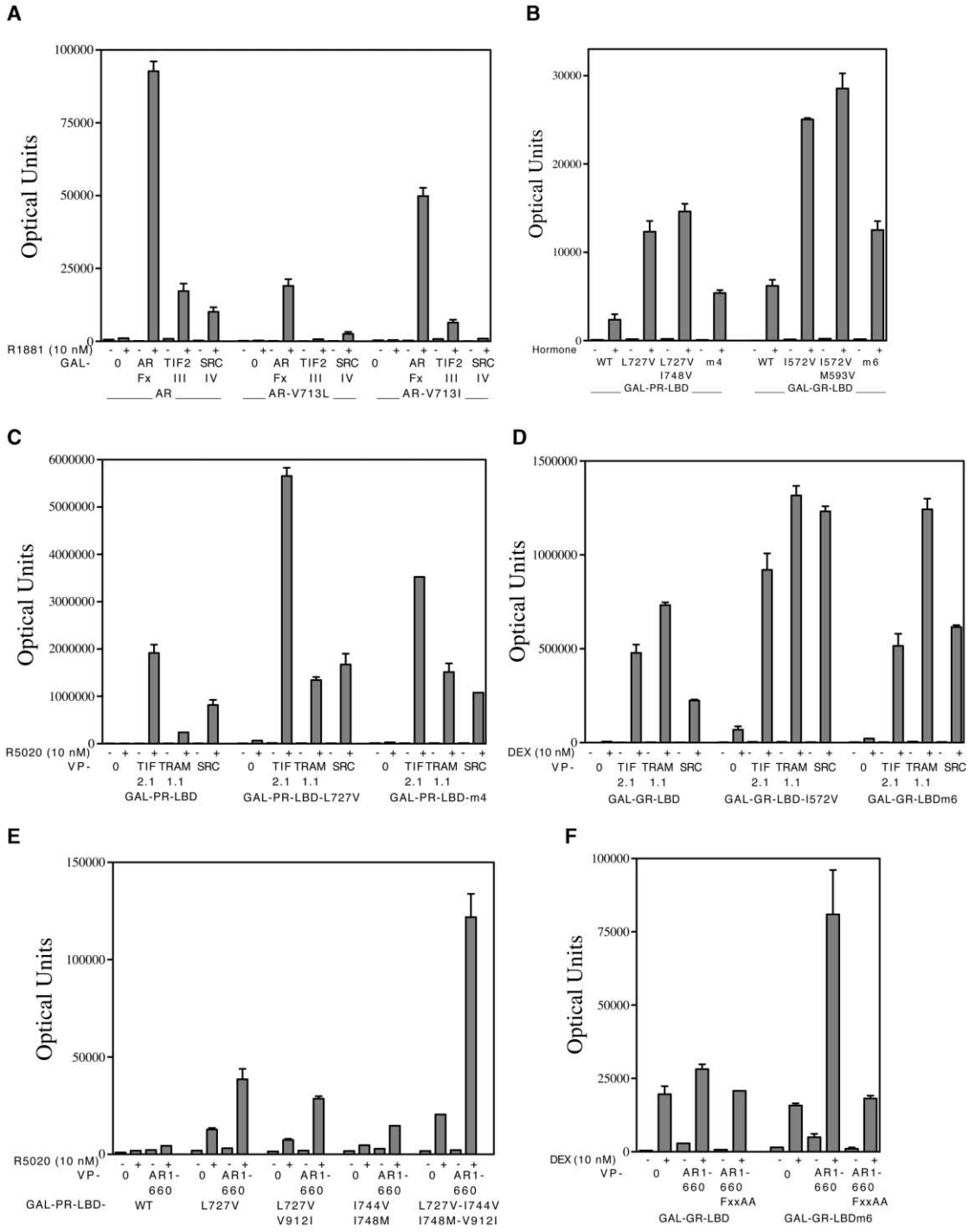

Figure 5. Evolutionary Decline in AF2 Activity and F*XX*LF Motif Binding by PR and GR Mutants

(A) Role of AR V713. Two-hybrid assays in HepG2 cells with and without 10 nM R1881 used 5×GAL4Luc3 and 5 ng/well pCMVhAR, AR-V713L, or V713I with 50 ng/well GAL0, GAL-AR20-30 (ARFx), GAL-TIF2-738-756 (TIF2-III), or GAL-SRC1-1428-1441 (SRC-IV).

(B) Inherent transcriptional activity of PR and GR AF2 mutants. HeLa cells were assayed using 50 ng/well GAL-PR-LBD (residues 636–933) or mutants L727V, L727V-I748V, or L727V-I744V-I748M-V912I (m4) with and without 1 nM R5020 or with 50 ng/well GAL-GR-LBD (residues 486–777) or mutants I572V, I572V-M593V, or G568E-V571L-I572V-A574V-L589V-L596I (m6) with and without 10 nM dexamethasone (DEX).

(C) Increase in L*XX*LL binding by PR AF2 mutants. Two-hybrid assays in HepG2 cells with or without 10 nM R5020 used 50 ng/well GAL-PR-LBD or mutants L727V or L727V-I744V-I748M-V912I (m4) with 50 ng/well pNLVP16 (0), VP-TIF2-624-1287 (TIF2.1), VP-TRAM1-604-1297 (TRAM1.1), or VP-SRC1-568-1441 (SRC).

(D) Increase in L*XX*LL binding by GR AF2 mutants. Two-hybrid assays in HepG2 cells with and without 10 nM DEX used 50 ng/well GAL-GR-LBD (residues 486–777) or mutants I572V or G568E-V571L-I572V-A574V-L589V-L596I (GR-LBDm6) with 50 ng/well VP-0, VP-TIF2.1, VP-TRAM1.1, or VP-SRC.

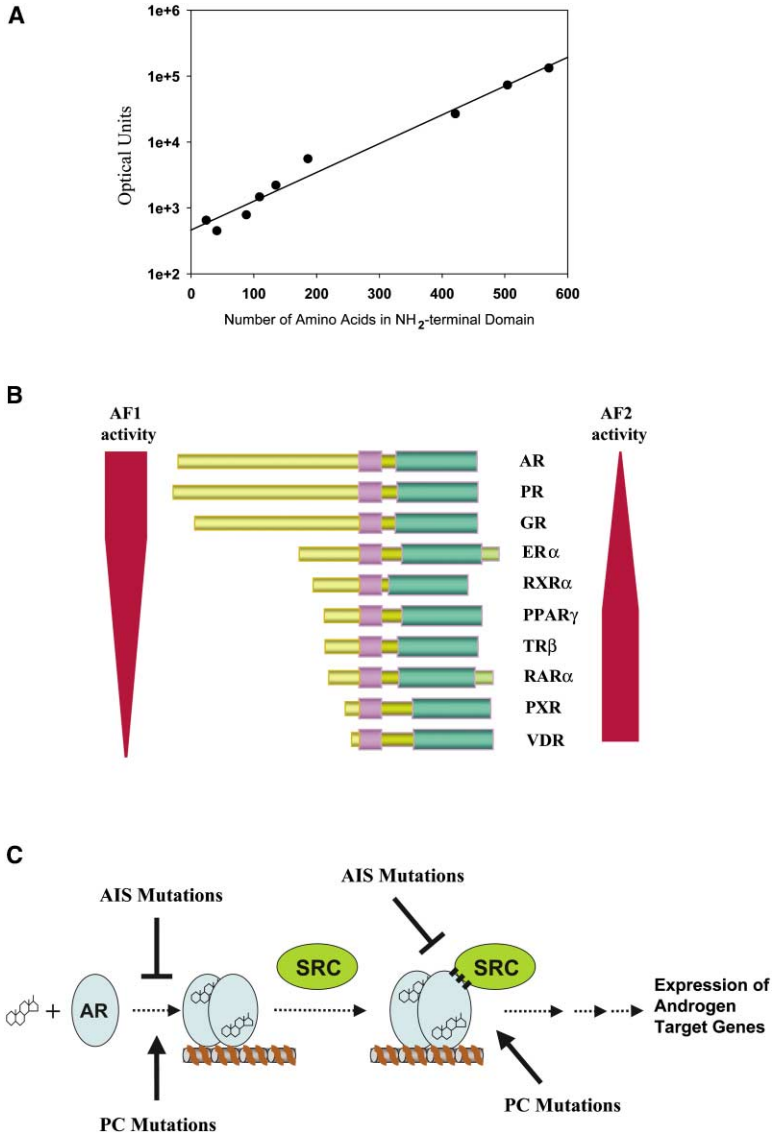

Figure 6. Direct Correlation between AF1 Activity and Length, and Models of NR Transactivation

(A) AF1 activity of NR NH_2-terminal regions. Human PRB1-569, AR1-503, GR1-420, ERα1-185, RXRα1-134, PPARγ1-108, RARα1-87, PXR1-40, and VDR1-23 expressed as GAL4 DNA binding domain fusion proteins (150 ng/well) were assayed in HepG2 cells using 5×GAL4Luc3.

(B) NR AF2 to AF1 transition. The data support an evolutionary transition from AF2 to AF1 as the dominant activation function from nonsteroid NRs to steroid receptors. Transition to AF1 parallels expansion and sequence diversity of the NH_2-terminal region. We speculate that the requirements for high-affinity hormone binding impose structural constraints on AF2 that limit evolutionary diversity in gene regulation. The NH_2-terminal region expands in length and functional significance during steroid receptor evolution. ER is intermediate between nonsteroid NRs and steroid receptors.

(C) Schematic of AR gene regulation. AR transactivation is inhibited by loss-of-function mutations that cause the androgen insensitivity syndrome (AIS). AR transactivation increases from gain-of-function mutations in prostate cancer (PC). An AR mutant in prostate cancer reverts to increased binding of SRC/p160 coactivators L*XX*LL motif.

shell. The 12 aromatic phenyl carbons in FQNLF present a larger hydrophobic contact surface than does L745 and L749 of TIF2-III. Conformational changes to AR M734 from F23 and F27 and M894 from L26 widens AF2 with F*XX*LF compared to L*XX*LL. The gap distance between M734 and M894 sulfur atoms is 10.4 Å for F*XX*LF, 8.4 Å for L*XX*LL, and 8.9 Å without peptide (Figure 2F). The narrower gap may reflect a poorer hydrophobic match between TIF2-III LRYLL and AR AF2 and may also contribute to the C-terminal shift and lost backbone H bonds to E897. Steric hindrance from a motif flanking residue such as L744(A) could also not be inferred due to the absence of electron density beyond the Cβ carbon. For the bound ^{23}FQNLF^{27}, specific enhancement of hydrophobic interactions may favorably position AR20-30 to H bond with E897 in helix 12. The F23 Cζ carbon lies ~1 Å closer to I737 in the AF2 floor than the TIF2-III L745 Cδ2 methyl in the bound ^{745}LRYLL^{749} structure. This orientation provides extensive and improved nonpolar contacts from F23 to Q738, L26 to M894 and V713, and from F27 to M734 and V730 in the helix 4 ridge.

Prominent roles of AR M734, V730, and V713 in F*XX*LF binding and recognition are supported by ligand dissociation studies. In the PR-like mutant AR-M734I, the smaller more rigid isoleucine increases ligand dissociation, suggesting important nonpolar interactions between M734 and F27 are altered. Faster ligand dissociation from the ER-like AR mutant V730L-M734V implies that the larger rigid leucine and smaller rigid valine at

(E) PR AF2 mutants bind AR F*XX*LF. Two-hybrid assays in HepG2 cells with and without 10 nM R5020 used 50 ng/well GAL-PR-636-933 (PR-LBD) or mutants L727V, L727V-V912I, I744V-I748M, or L727V-I744V-I748M-V912I with 50 ng/well pNLVP16 (VP-0) or VP-AR1-660.

(F) GR AF2 mutants bind AR F*XX*LF. Two-hybrid assays in HepG2 cells with and without 10 nM DEX used 50 ng/well GAL-GR486-777 (GR-LBD) or mutant G568E-V571L-I572V-A574V-L589V-L596I (GR-LBDm6) with 50 ng/well VP-0, VP-AR1-660, or VP-AR1-660-F*XX*AA.

F27 destabilize FQNLF interactions with AF2. Slightly faster ligand dissociation rates also occur for PR-like mutant AR-V730I-M734I. Increased binding of L*XX*LL by these AR mutants indicates M734 and V730 contribute to peptide recognition.

The contribution of V730 to F*XX*LF recognition is further explained by the small valine side chain that accommodates the bulky F27, establishing good complementary shape and distance separation. In contrast, ER, PR, and GR have the larger isoleucine or leucine relative to AR V730, preferentially binding L*XX*LL with its smaller i+5 leucine. The even larger methionine in the AR prostate cancer mutant V730M improves L*XX*LL binding but does not greatly affect F*XX*LF binding. The flexible methionine side chain may improve hydrophobic interactions when presented with an i+5 leucine from L*XX*LL or adapt to an i+5 phenylalanine from F*XX*LF. From the crystal structures, sufficient space accommodates the various conformations of a methionine side chain that could account for this exception. Mismatching F*XX*LF to a receptor with larger, rigid isoleucine or leucine could also lead to unfavorable contacts between side chains. Reduced interaction between F*XX*LF and AR V713L or V713I that mimic PR and GR likely result from unfavorable interactions between the i+4 L26 and the larger mutated side chain. The data indicate AR M734, V730, and V713 contribute to F*XX*LF recognition and preference through optimized residue matching and complementary hydrophobic shape.

Other regions of the LBD impose allosteric effects on coactivator binding depending on the bound ligand (Shulman et al., 2004; Nettles et al., 2004). AR favors F*XX*LF binding when bound to DHT and L*XX*LL with the partial agonist androstenedione (Gregory et al., 2001). When AR V730 and M734 are changed to corresponding residues in PR and ER, AR binding of SRC1 and TIF2 increases in the presence of high-affinity agonists. However, transcriptional activities of the AR mutants remain weak compared to PR or GR. Activities of PR and GR LBDs are greater than the AR LBD when mutated at multiple sites to mimic the AR AF2 surface, suggesting additional determinants of NR AF2 activity.

AR AF2 preferentially binds F*XX*LF and other steroid receptors bind L*XX*LL (Heery et al., 1997), but AF2 binding is not exclusive to a single motif. We show that AR binds coactivator L*XX*LL motifs with weaker affinity than F*XX*LF but can bind artificial L*XX*LL peptides with higher affinity (Chang et al., 1999). Mutated PR and GR AF2 bind both F*XX*LF and L*XX*LL motifs. Adaptability of AF2 is supported by variant sequences F*XX*LL (Huang et al., 1998) and L*XX*IL (Li et al., 1999) that mediate coregulators interactions.

Evolutionary Decline in AF2 Activity

Weak transactivation by AR AF2 (He et al., 1999) results from evolving sequence changes that reduce L*XX*LL binding. Concurrently, AR F*XX*LF evolved with the expanding NH_2-terminal AF1 and avidly binds AF2, further limiting coactivator recruitment by competitive binding at AF2 (He et al., 2001) (Figure 6B). We show that evolving sequence changes also decrease L*XX*LL binding by PR and GR AF2, with increasing size and functional importance of AF1 (Sartorius et al., 1994). Evolutionarily older nonsteroid NRs such as RXR and RAR also tend toward NH_2-terminal expansion and increased AF1 activity, although AF2 typically predominates (Nagpal et al., 1993). ERα is evolutionarily intermediate between nonsteroid and steroid receptors (Thornton, 2001) with intermediate NH_2-terminal length and cell-type-dependent AF1 and AF2 activities (Metzger et al., 1992; Tremblay et al., 1999). Orphan NRs can also have extensive NH_2-terminal regions with potent AF1 activity. AF1 of Nurr1 mediates strong autonomous transactivation in various cells (Nordzell et al., 2004), whereas transactivation by its LBD is cell-type dependent (Castro et al., 1999). Thus, evolving NH_2-terminal domains occur among liganded and orphan NRs.

Sequence diversity in the NH_2-terminal region contrasts the conserved LBDs, where the structural constraints of high-affinity hormone binding limit the binding surfaces to L*XX*LL and F*XX*LF-like motifs. Evolution of AF1 as the dominant activation domain can provide unique interaction sites for tissue and species-specific coregulators. Such diversification can increase specificity in gene regulation by AR, PR, GR, and the mineralocorticoid receptor, which bind similar DNA response elements. Our hypothesis for an AF2 to AF1 switch in dominant activation domain also allows for increased diversity in gene regulation between receptor isoforms. In contrast to PR-B, PR-A is less active and can function as a repressor through progesterone and estrogen signaling pathways, allowing progesterone to activate and repress gene transcription through separate isoforms of the same receptor. In this case, the PR LBD functions more like a regulatory domain than a transactivation domain.

The hormone requirement for AR and GR DNA binding may minimize inappropriate gene activity by the evolving AF1. This contrasts nonsteroid NRs for vitamin D, thyroid hormone, and retinoic acid that have weaker AF1 activity, and in the absence of hormone, bind DNA and recruit corepressors to actively repress transcription. Sequestering steroid receptors by heat shock proteins further minimizes inadvertent gene activation by AF1 in the absence of hormone. For ERα in the absence of hormone, an NH_2-terminal A domain LL*XX*I helix competes with the corepressor for a hydrophobic cleft in the LBD to maintain ERα in an inactive state (Metivier et al., 2002).

Selective Advantage in Prostate Cancer

Increased AR activity in prostate cancer is associated with increased levels of AR (Visakorpi et al., 1995) and SRC/p160 coactivators, and autocrine signaling (Gregory et al., 2004). Functional AR mutations tend to appear after antiandrogen or androgen withdrawal therapy (Gelmann, 2002) and contrast loss-of-function mutations that cause androgen insensitivity (Quigley et al., 1995) (Figure 6C). AR transactivation is typically retained in prostate cancer and for some mutants, transactivation increases with different steroids (Culig et al., 1993; Peterziel et al., 1995; Tan et al., 1997).

Here we link an AR somatic prostate cancer mutation to increased L*XX*LL motif binding and SRC coactivator recruitment. AR-V730M retains high-affinity binding of DHT and increased transcriptional activity by adrenal androgens (Newmark et al., 1992; Culig et al., 1993;

Peterziel et al., 1995) (data not shown). V730M increases L*XX*LL binding without reducing F*XX*LF binding and could impact early and late stage cancer. Increased coactivator recruitment by a somatic mutation is a mechanism for aberrant gene regulation that could provide a selective growth advantage to prostate cancer cell survival.

Experimental Procedures

Protein Preparation

NH_2-terminal 6×His-tagged human AR LBD residues 663–919 with a thrombin protease site was expressed from pET15b in *E. coli* Bl21DE3. Cells were grown overnight at 17°C in nutrient-rich media amended with 5 μM R1881 and 1 mM isopropyl-thiogalactopyranoside. Overnight thrombin digestion (5 NIH units/mg protein) at 4°C was performed on pooled, immobilized metal affinity chromatography-purified fractions prior to cation exchange and gel filtration chromatography. The dilute binary complex in 25 mM HEPES (pH 7.5), 0.5 M NaCl, 5 mM DTT, 0.5 mM EDTA, 0.05% β-n-octoglucoside, 10% glycerol, and 10 μM R1881 was used or amended with 2- to 3-fold molar excess of AR 20-30 peptide RGAFQNLFQSV (He et al., 2002b). The dilute binary complex dissolved in 25 mM HEPES (pH 7.5), 0.15 M Li_2SO_4, 10 mM DTT, 0.5 mM EDTA, 0.05% β-n-octoglucoside, 10% glycerol, and 10 μM R1881 was amended with 2- to 3-fold molar excess of TIF2-740-753 L*XX*LL-III peptide KENALLRYLLDKDD (Voegel et al., 1998). Samples were filtered and concentrated to 2–3 mg/ml prior to crystallization.

Crystallization and Data Collection

All crystals grew at 20°C to ~150 μM in 2 weeks by vapor diffusion using a 1:1 (v/v) ratio of complex to well solution. Well solution for AR LBD-R1881 with and without AR 20-30 contained 100 mM Bis-Tris propane (pH 7.5 or 8.5), with a 0.6–1.2 M gradient of lithium sulfate. For TIF2-III 740-753 complexes, a solution containing 100 mM Bis-Tris propane (pH 7.9) and 0.6 M Na/K tartrate was used. Well solutions with 20% glycerol were used to transiently mix the crystals prior to flash freezing in liquid N_2. X-ray diffraction data were collected at −180°C with a MAR-345 detector on a Rigaku RU-H-2R-200 generator, an ADSC 210 detector at the IMCA-CAT, sector 17ID or MARCCD at sector 32ID at the Advanced Photon Source. The observed reflections were processed with the HKL2000 package (Otwinowski and Minor, 1997).

Structure Determination and Refinement

The AR-DHT structure (Sack et al., 2001) (access code 1I37) yielded a convincing AMoRe (Navaza, 2001) molecular replacement solution with one AR LBD complex in the asymmetric unit. Multiple cycles of manual model building were completed with QUANTA (Accelrys, Inc.) and refined with CNX (Accelrys, Inc.) (Brunger, et al., 1998). Initial AR-R1881 and AR-R1881-TIF2 structures were determined from the final AR-R1881-AR 20-30 LBD structure, followed by iterative building and refinement with CNX. Table 1 summarizes the crystallographic and structure refinement statistics. Superimpositions were performed using the homology modeling package in Insight (Accelrys, Inc.). Figures 1 and 2C–2F were generated with PyMol from Delano Scientific (www.pymol.org).

Cell Transfections and Biochemical Measurements

Peptide binding affinities were determined by fluorescence polarization (Stanley et al., 2003) using 40 μM R1881 and 17β-estradiol and 10 nM AR 20-30 (fluorescein-RGAFQNLFQSV) and TIF2-III 740-751 (fluoroscein-KENALLRYLLDK). GAL4-DNA binding domain and VP16 activation domain fusion peptides were prepared (He et al., 2002b). AR transcriptional activity and two-hybrid interaction assays were by transfection of HepG2 and HeLa cells in 12 well tissue culture plates using Effectene (Qiagen). MMTV-Luc, PSA-Enh-Luc (Huang et al., 1999), and p21-Luc (Lu et al., 1999) were used at 0.25 μg/well and 5×GAL4Luc3 at 0.1 μg/well (He and Wilson, 2003). Cells were incubated with and without hormones for 24 hr at 37°C and luciferase activity measured (He et al., 2001). GST fusion proteins and ^{35}S-methionine in vitro translated AR LBD (pcDNA3-HA-AR624-919) were analyzed (He et al., 2002a). Apparent equilibrium binding and dissociation rate studies of [^{3}H]R1881 were determined after transient expression in COS cells (He et al., 2001).

Acknowledgments

The work was supported by Public Health Service Grant HD16910 and cooperative agreement U54-HD35014 of the Specialized Cooperative Center Program in Reproductive Research from NICHD, P01-CA77739 from NCI, and NIH Fogarty International Center grant R03TW001234 to Frank S. French. X-ray diffraction data collected at the Industrial Macromolecular Crystallography Association-Collaborative Access Team (IMCA-CAT) of the Advanced Photon Source are supported by companies of the IMCA-CAT under contract with the Illinois Institute of Technology (IIT), executed through the IIT Center for Synchrotron Radiation Research and Instrumentation. Use of the Advanced Photon Source is supported by the US Department of Energy, Basic Energy Sciences, Office of Science, under Contract No. W-31-109-Eng-38.

Received: April 22, 2004
Revised: July 26, 2004
Accepted: August 26, 2004
Published: November 4, 2004

References

Bledsoe, R.K., Montana, V.G., Stanley, T.B., Delves, C.J., Apolito, C.J., McKee, D.D., Consler, T.G., Parks, D.J., Stewart, E.L., Willson, T.M., et al. (2002). Crystal structure of the glucocorticoid receptor ligand binding domain reveals a novel mode of receptor dimerization and coactivator recognition. Cell *110*, 93–105.

Brunger, A.T., Adams, P.D., Clore, G.M., DeLano, W.L., Gros, P., Grosse-Kunstleve, R.W., Jiang, J.S., Kuszewski, J., Nilges, M., Pannu, N.S., et al. (1998). Crystallography and NMR system: a new software suite for macromolecular structure determination. Acta Crystallogr. D Biol. Crystallogr. *54*, 905–921.

Castro, D.S., Arvidsson, M., Bondesson Bolin, M., and Perlmann, T. (1999). Activity of the Nurr1 carboxyl-terminal domain depends on cell type and integrity of the activation function 2. J. Biol. Chem. *274*, 37483–37490.

Chang, C., Norris, J.D., Gron, H., Paige, L.A., Hamilton, P.T., Kenan, D.J., Fowlkes, D., and McDonnell, D.P. (1999). Dissection of the L*XX*LL nuclear receptor-coactivator interaction motif using combinatorial peptide libraries: discovery of peptide antagonists of estrogen receptors alpha an beta. Mol. Cell. Biol. *19*, 8226–8239.

Chawla, A., Repa, J.J., Evans, R.M., and Mangelsdorf, D.J. (2001). Nuclear receptors and lipid physiology: opening the X-files. Science *294*, 1866–1870.

Culig, Z., Hobisch, A., Cronauer, M.V., Cato, A.C., Hittmair, A., Radmayr, C., Eberle, J., Bartsch, G., and Klocker, H. (1993). Mutant androgen receptor detected in an advanced-stage prostatic carcinoma is activated by adrenal androgens and progesterone. Mol. Endocrinol. *7*, 1541–1550.

Darimont, B.D., Wagner, R.L., Apriletti, J.W., Stallcup, M.R., Kushner, P.J., Baxter, J.D., Fletterick, R.J., and Yamamoto, K.R. (1998). Structure and specificity of nuclear receptor-coactivator interactions. Genes Dev. *12*, 3343–3356.

Gampe, R.T., Jr., Montana, V.G., Lambert, M.H., Miller, A.B., Bledsoe, R.K., Milburn, M.V., Kliewer, S.A., Willson, T.M., and Xu, E.X. (2000). Asymmetry in the PPARγ/RXRα crystal structure reveals the molecular basis of heterodimerization among nuclear receptors. Mol. Cell *5*, 545–555.

Gelmann, E.P. (2002). Molecular biology of the androgen receptor. J. Clin. Oncol. *20*, 3001–3015.

Glass, C.K., and Rosenfeld, M.G. (2000). The coregulator exchange in transcriptional functions of nuclear receptors. Genes Dev. *14*, 121–141.

Gregory, C.W., He, B., Johnson, R.T., Ford, O.H., Mohler, J.L., French, F.S., and Wilson, E.M. (2001). A mechanism for androgen receptor mediated prostate cancer recurrence after androgen deprivation therapy. Cancer Res. *61*, 4315–4319.

Gregory, C.W., Fei, X., Ponguta, L.A., He, B., Bill, H.M., French, F.S., and Wilson, E.M. (2004). Epidermal growth factor increases coactivation of the androgen receptor in recurrent prostate cancer. J. Biol. Chem. *279*, 7119–7130.

He, B., and Wilson, E.M. (2003). Electrostatic modulation of steroid receptor recruitment of the L*XX*LL and F*XX*LF motifs. Mol. Cell. Biol. *23*, 2135–2150.

He, B., Kemppainen, J.A., Voegel, J.J., Gronemeyer, H., and Wilson, E.M. (1999). Activation function 2 in the human androgen receptor ligand binding domain mediates interdomain communication with the NH_2-terminal domain. J. Biol. Chem. *274*, 37219–37225.

He, B., Kemppainen, J.A., and Wilson, E.M. (2000). F*XX*LF and W*XX*LF sequences mediate the NH_2-terminal interaction with the ligand binding domain of the androgen receptor. J. Biol. Chem. *275*, 22986–22994.

He, B., Bowen, N.T., Minges, J.T., and Wilson, E.M. (2001). Androgen-induced NH_2- and COOH-terminal interaction inhibits p160 coactivator recruitment by activation function 2. J. Biol. Chem. *276*, 42293–42301.

He, B., Lee, L.W., Minges, J.T., and Wilson, E.M. (2002a). Dependence of selective gene activation on the androgen receptor NH_2- and carboxyl-terminal interaction. J. Biol. Chem. *277*, 25631–25639.

He, B., Minges, J.T., Lee, L.W., and Wilson, E.M. (2002b). The F*XX*LF motif mediates androgen receptor-specific interactions with coregulators. J. Biol. Chem. *277*, 10226–10235.

Heery, D.M., Kalkhoven, E., Hoare, S., and Parker, M.G. (1997). A signature motif in transcriptional co-activators mediates binding to nuclear receptors. Nature *387*, 733–736.

Hong, H., Kohli, K., Trivedi, A., Johnson, D.L., and Stallcup, M.R. (1996). GRIP1, a novel mouse protein that serves as a transcriptional coactivator in yeast for the hormone binding domains of steroid receptors. Proc. Natl. Acad. Sci. USA *93*, 4948–4952.

Hsu, C.L., Chen, Y.L., Yeh, S., Ting, H.J., Hu, Y.C., Lin, H., Wang, X., and Chang, C. (2003). The use of phage display technique for the isolation of androgen receptor interacting peptides with (F/W)*XX*L(F/W) and F*XX*LY new signature motifs. J. Biol. Chem. *278*, 23691–23698.

Huang, N., vom Baur, E., Garnier, J.M., Lerouge, T., Vonesch, J.L., Lutz, Y., Chambon, P., and Losson, R. (1998). Two distinct nuclear receptor interaction domains in NSD1, a novel SET protein that exhibits characteristics of both corepressors and coactivators. EMBO J. *17*, 3398–3412.

Huang, W., Shostak, Y., Tarr, P., Sawyers, C., and Carey, M. (1999). Cooperative assembly of androgen receptor into a nucleoprotein complex that regulates the prostate-specific antigen enhancer. J. Biol. Chem. *274*, 25756–25768.

Langley, E., Kemppainen, J.A., and Wilson, E.M. (1998). Intermolecular NH_2-/carboxyl-terminal interactions in androgen receptor dimerization revealed by mutations that cause androgen insensitivity. J. Biol. Chem. *273*, 92–101.

Li, D., Desai-Yajnik, V., Lo, E., Schapira, M., Abagyan, R., and Samuels, H.H. (1999). NRIF3 is a novel coactivator mediating functional specificity of nuclear hormone receptors. Mol. Cell. Biol. *19*, 7191–7202.

Lu, S., Liu, M., Epner, D.E., Tsai, S.Y., and Tsai, M.J. (1999). Androgen regulation of the cyclin-dependent kinase inhibitor p21 gene through an androgen response element in the proximal promoter. Mol. Endocrinol. *13*, 376–384.

Matias, P.M., Donner, P., Coelho, R., Thomaz, M., Peixoto, C., Macedo, S., Otto, N., Joschko, S., Scholz, P., Wegg, A., et al. (2000). Structural evidence for ligand specificity in the binding domain of the human androgen receptor. Implications for pathogenic gene mutations. J. Biol. Chem. *275*, 26164–26171.

Metivier, R., Stark, A., Flouriot, G., Hubner, M.R., Brand, H., Penot, G., Manu, D., Denger, S., Reid, G., Kos, M., et al. (2002). A dynamic structural model for estrogen receptor-alpha activation by ligands, emphasizing the role of interactions between distant A and E domains. Mol. Cell *10*, 1019–1032.

Metzger, D., Losson, R., Bornert, J.M., Lemoine, Y., and Chambon, P. (1992). Promoter specificity of the two transcriptional activation functions of the human oestrogen receptor in yeast. Nucleic Acids Res. *20*, 2813–2817.

Moras, D., and Gronemeyer, H. (1998). The nuclear receptor ligand-binding domain: structure and function. Curr. Opin. Cell Biol. *10*, 384–391.

Nagpal, S., Friant, S., Nakshatri, H., and Chambon, P. (1993). RARs and RXRs: evidence for two autonomous transactivation functions (AF-1 and AF-2) and heterodimerization *in vivo*. EMBO J. *12*, 2349–2360.

Navaza, J. (2001). AMoRe: implementation of molecular replacement in AMoRe. Acta Crystallogr. D. Biol. Crystallogr. *57*, 1367–1372.

Nettles, K.W., Sun, J., Radek, J.T., Sheng, S., Rodriguez, A.L., Katzenellenbogen, J.A., Katzenellenbogen, B.S., and Greene, G.L. (2004). Allosteric control of ligand selectivity between estrogen receptors α and β: implications for other nuclear receptors. Mol. Cell *13*, 317–327.

Newmark, J.R., Hardy, D.O., Tonb, D.C., Carter, B.S., Epstein, J.I., Isaacs, W.B., Brown, T.R., and Barrack, E.R. (1992). Androgen receptor gene mutations in human prostate cancer. Proc. Natl. Acad. Sci. USA *89*, 6319–6323.

Nolte, R.T., Wisely, G.B., Westin, S., Cobb, J.E., Lambert, M.H., Kurokawa, R., Rosenfeld, M.G., Willson, T.M., Glass, C.K., and Milburn, M.V. (1998). Ligand binding and co-activator assembly of the peroxisome proliferator-activated receptor-gamma. Nature *395*, 137–143.

Nordzell, M., Aarnisalo, P., Benoit, G., Castro, D.S., and Perlmann, T. (2004). Defining an N-terminal activation domain of the orphan nuclear receptor Nurr1. Biochem. Biophys. Res. Commun. *313*, 205–211.

Ogryzko, V.V., Schiltz, R.L., Russanova, V., Howard, B.H., and Nakatani, Y. (1996). The transcriptional coactivators p300 and CBP are histone acetyltransferases. Cell *87*, 953–959.

Onate, S.A., Tsai, S.Y., Tsai, M.J., and O'Malley, B.W. (1995). Sequence and characterization of a coactivator for the steroid hormone receptor superfamily. Science *270*, 1354–1357.

Otwinowski, Z., and Minor, W. (1997). Processing of x-ray diffraction data collected in oscillation mode. Methods Enzymol. *276*, 307–326.

Peterziel, H., Culig, Z., Stober, J., Hobisch, A., Radmayr, C., Bartsch, G., Klocker, H., and Cato, A.C. (1995). Mutant androgen receptors in prostatic tumors distinguish between amino-acid-sequence requirements for transactivation and ligand binding. Int. J. Cancer *63*, 544–550.

Quigley, C.A., De Bellis, A., Marschke, K.B., El-Awady, M.K., Wilson, E.M., and French, F.S. (1995). Androgen receptor defects: historical, clinical and molecular perspectives. Endocr. Rev. *16*, 271–321.

Sack, J.S., Kish, K.F., Wang, C., Attar, R.M., Kiefer, S.E., An, Y., Wu, G.Y., Scheffler, J.E., Salvati, M.E., Krystek, S.R., Jr., et al. (2001). Crystallographic structures of the ligand-binding domains of the androgen receptor and its T877A mutant complexed with the natural agonist dihydrotestosterone. Proc. Natl. Acad. Sci. USA *98*, 4904–4909.

Sartorius, C.A., Melville, M.Y., Hovland, A.R., Tung, L., Takimoto, G.S., and Horwitz, K.B. (1994). A third transactivation function (AF3) of human progesterone receptors located in the unique N-terminal segment of the B-isoform. Mol. Endocrinol. *8*, 1347–1360.

Shiau, A.K., Barstad, D., Loria, P.M., Cheng, L., Kushner, P.J., Agard, D.A., and Greene, G.L. (1998). The structural basis of estrogen receptor/coactivator recognition and the antagonism of this interaction by tamoxifen. Cell *95*, 927–937.

Shulman, A.I., Larson, C., Mangelsdorf, D.J., and Rama, R. (2004). Structural determinants of allosteric ligand activation in RXR heterodimers. Cell *116*, 417–429.

Stanley, T.B., Leesnitzer, L.M., Montana, V.G., Galardi, C.M., Lambert, M.H., Holt, J.A., Xu, H.E., Moore, L.B., Blanchard, S.G., and Stimmel, J.B. (2003). Subtype specific effects of peroxisome proliferator-activated receptor ligands on corepressor affinity. Biochemistry *42*, 9278–9287.

Tan, J., Sharief, Y., Hamil, K.G., Gregory, C.W., Zang, D.Y., Sar, M.,

Gumerlock, P.H., deVere White, R.W., Pretlow, T.G., Harris, S.E., et al. (1997). Dehydroepiandrosterone activates mutant androgen receptors expressed in the androgen-dependent human prostate cancer xenograft CWR22 and LNCaP cells. Mol. Endocrinol. *11*, 450–459.

Thornton, J.W. (2001). Evolution of vertebrate steroid receptors from an ancestral estrogen receptor by ligand exploitation and serial genome expansions. Proc. Natl. Acad. Sci. USA *98*, 5671–5676.

Tremblay, G.B., Tremblay, A., Labrie, F., and Giguere, V. (1999). Dominant activity of activation function 1 (AF-1) and differential stoichiometric requirements for AF-1 and -2 in the estrogen receptor alpha-beta heterodimeric complex. Mol. Cell. Biol. *19*, 1919–1927.

Tsai, M.J., and O'Malley, B.W. (1994). Molecular mechanisms of action of steroid/thyroid receptor superfamily members. Annu. Rev. Biochem. *63*, 451–486.

Visakorpi, T., Hyytinen, E., Koivisto, P., Tanner, M., Keinanen, R., Palmberg, C., Palotie, A., Tammela, T., Isola, J., and Kallioniemi, O.P. (1995). In vivo amplification of the androgen receptor gene and progression of human prostate cancer. Nat. Genet. *9*, 401–406.

Voegel, J.J., Heine, M.J., Tini, M., Vivat, V., Chambon, P., and Gronemeyer, H. (1998). The coactivator TIF2 contains three nuclear receptor-binding motifs and mediates transactivation through CBP binding-dependent and -independent pathways. EMBO J. *17*, 507–519.

Webster, N.J., Green, S., Tasset, D., Ponglikitmongkol, M., and Chambon, P. (1989). The transcriptional activation function located in the hormone-binding domain of the human oestrogen receptor is not encoded in a single exon. EMBO J. *8*, 1441–1446.

Williams, S.P., and Sigler, P.B. (1998). Atomic structure of progesterone complexed with its receptor. Nature *378*, 392–396.

Accession Numbers

The Protein Data Bank (http://www.rcsb.org/pdb) accession numbers for the crystal structures presented here are 1XOW (FXXLF), 1XQ2 (LXXLL), and 1XQ3 (no peptide).